Structural, Magnetic, and Dynamic Characterization of the $(d_{xz},d_{yz})^4(d_{xy})^1$ Ground-State Low-Spin Iron(III) Tetraphenylporphyrinate Complex [(*p*-TTP)Fe(2,6-XylylNC)$_2$]CF_3SO_3

Gérard Simonneaux,*,† Volker Schünemann,‡ Christophe Morice,† Laurence Carel,† Loïc Toupet,§ Heiner Winkler,‡ Alfred X. Trautwein,*,‡ and F. Ann Walker*,⊥

Contribution from the Laboratoire de Chimie Organométallique et Biologique, UMR CNRS 6509, Université de Rennes 1, Campus de Beaulieu, 35042 Rennes Cedex, France, Institut für Physik, Medizinische Universität zu Lübeck, 160 Ratzeburger Allee, D-23538 Lübeck, Germany, Groupe de Physique Cristalline, UA CNRS 040804, Université de Rennes 1, Campus de Beaulieu, 35042 Rennes Cedex, France, and Department of Chemistry, University of Arizona, Tucson, Arizona 85721-0041

Received November 30, 1999

Abstract: The synthesis and characterization of the trifluoromethanesulfonate salt of bis(2,6-xylyl isocyanide)-tetrakis(*p*-tolyl)porphyrinatoiron(III), [(*p*-TTP)Fe(2,6-xylylNC)$_2$]CF_3SO_3 (**1**), is reported. The crystal structure shows that the porphyrinate ring is strongly ruffled. The equatorial Fe−N bond distances average to 1.961(7) Å for **1**, which is quite short for low-spin iron(III) porphyrinate derivatives. Two additional complexes, having TPP (**2**) and *m*-TTP (**3**) as the porphyrinates, were also synthesized and studied by NMR, EPR, and Mössbauer spectroscopy. All physical properties are consistent with a low-spin iron(III) porphyrinate with the less-common ground-state configuration $(d_{xz},d_{yz})^4(d_{xy})^1$. The ^{1}H NMR chemical shift of the pyrrole protons at 297 K is +10.7 ppm for **1**. The EPR spectrum of **1** in solution is axial, with $g_\perp = 2.15$ and $g_{||} = 1.94$, $\sum g^2 = 13.0$, while in the solid state $g_\perp = 2.2$ and $g_{||} = 1.94$, $\sum g^2 = 13.4$. The Mössbauer spectrum of **1** at 190 K has an isomer shift of 0.14 mm/s and quadrupole splitting of 1.81 mm/s. Magnetic Mössbauer spectra analyzed in the intermediate spin−spin relaxation regime by the dynamic line-shape formalism of Blume and Clauser confirm this electron configuration and yield large negative quadrupole splittings, $\Delta E_Q = -1.8$ to -2.0 mm/s for the three complexes. To our knowledge, this is the first case in which the Mössbauer spectra of low-spin ferriheme systems have been analyzed in terms of the effect of intermediate rates of spin fluctuations on the appearance of the spectra. Analysis of the temperature dependence of the quadrupole splitting, ΔE_Q, for **2** yielded a different estimate of the energy separation between the $(d_{xz},d_{yz})^4(d_{xy})^1$ ground state and an excited state than did the temperature dependence of the NMR isotropic shifts. It is postulated that the excited state is actually the planar transition state between the two ruffled conformations of the porphyrinate that are related by "inversion". To explain the temperature dependence of both NMR isotropic shifts and Mössbauer quadupole splittings, the planar transition state must have the $(d_{xy})^2(d_{xz},d_{yz})^3$ electron configuration. The energy barrier appears to be smaller in homogeneous solution than in the solid state and is considerably lower than that predicted for the $(d_{xz},d_{yz})^3(d_{xy})^2$ excited electronic state of the ruffled conformation on the basis of the EPR *g* values.

Introduction

Investigations of the structural and spectroscopic properties of Fe(III) porphyrinates have been useful in understanding both structural and electronic properties of the bis-histidine-coordinated cytochromes b_5[1] and c_3,[2,3] as well as the membrane-bound cytochromes *b* with bis(histidine) coordination[4,5] including the two *b* cytochromes of mitochondrial "complex III" (also known as ubiquinone-cytochrome *c* oxidoreductase) and chloroplast cytochrome b_6. EPR spectroscopy,[6] and in some cases Mössbauer spectroscopy,[7] of well-defined low-spin heme model compounds with high basicity pyridines, imidazoles, or cyanides as the axial ligands has shown that their "large g_{max}" EPR signal is indicative of the $(d_{xy})^2(d_{xz},d_{yz})^3$ electronic ground state and near degeneracy of d_{xz} and d_{yz}. For complexes with planar axial ligands this correlates with perpendicular alignment of these ligands,[7−10] while rhombic EPR signals are correlated with parallel alignment of planar axial ligands.

Tetraphenylporphinatoiron(III) bis(4-cyanopyridine)perchlorate, [(TPP)Fe(4-CNPy)$_2$]ClO_4,[11] for which the axial ligands

† Laboratoire de Chimie Organométallique et Biologique, Université de Rennes 1.
‡ Medizinische Universität zu Lübeck.
§ Groupe de Physique Cristalline, UA CNRS 040804, Université de Rennes 1.
⊥ University of Arizona.

(1) Mathews, F. S.; Czerwinski, E. W.; Argos. P. In *The Porphyrins*; Dolphin, D., Ed.; Academic Press: New York, 1979; Vol. VIII, p 108.
(2) Pierrot, M.; Haser, R.; Frey, M.; Payan, F.; Astier, J.-P. *J. Biol. Chem.* **1982**, *257*, 14341.
(3) Higuchi, Y.; Kusunocki, M.; Matsuura, Y.; Yasuoka, N.; Kakudo M. *J. Mol. Biol.* **1984**, *172*, 109.
(4) Widger, W. R.; Cramer, W. A.; Herrmann, R. G.; Trebst, A. *Proc. Natl. Acad. Sci. U.S.A.* **1984**, *81*, 674.
(5) Babcock, G. T.; Widger, W. R.; Cramer, W. A.; Oertling, W. A.; Metz, J. *Biochemistry* **1985**, *24*, 3638.
(6) Innis, D.; Soltis, S. M.; Strouse, C. E. *J. Am. Chem. Soc.* **1988**, *110*, 5644.
(7) Walker, F. A.; Huynh, B. H.; Scheidt, W. R.; Osvath, S. R. *J. Am. Chem. Soc.* **1986**, *108*, 5288.

10.1021/ja994190t CCC: $19.00
Published on Web 04/25/2000

have strong π-acceptor properties, has been shown to have an electronic stabilization of the $(d_{xz},d_{yz})^4(d_{xy})^1$ electronic ground state. The corresponding tetramesitylporphyrinate, [(TMP)Fe(4-CNPy)$_2$]ClO$_4$,[12] also reveals properties such as low-intensity visible[13] and near-IR[14] MCD bands, as well as EPR *g* values that resemble those of iron chlorins[15] and proteins that contain them.[15,16] A Mössbauer, EPR, and NMR study of the *tert*-butyl isocyanide complexes, [(TPP)Fe(*t*-BuNC)$_2$]ClO$_4$ and [(OEP)Fe(*t*-BuNC)$_2$]ClO$_4$,[17] has shown that their *g* values ($g_\perp = 2.20-2.28$, $g_{||} = 1.94-1.83$) are consistent with the purest $(d_{xz},d_{yz})^4(d_{xy})^1$ ground-state systems observed thus far, with the most complete quenching of orbital momentum ($\sum g^2$ as small as 13.5). Thus, it is now apparent that iron(III) tetraphenylporphyrinates, when bound to strong π-acceptor ligands, are good models of the "green hemes" that include (i) the iron chlorin that is the prosthetic group of hydroperoxidase II[18] and cytochrome *bd*[19] from *Escherichia coli*, (ii) the iron dioxoisobacteriochlorin of heme d_1, the prosthetic group of the dissimilatory nitrite reductase of denitrifying bacteria,[20] and (iii) the siroheme prosthetic group of bacterial sulfite and nitrite reductases.[21]

The relative energies of the d_{xy}, d_{xz} and d_{yz} orbitals can be calculated from the EPR *g* values on the basis of Griffith's theory[22] by adopting the methods and "proper axis system" of Taylor.[23] For the complexes showing the "large g_{max}" EPR signal, Mössbauer spectroscopy has been used to estimate the components of the *g*-tensor which are not observable by EPR.[7,9] Mössbauer spectroscopy in high magnetic fields and at low temperatures also allows determination of the sign of the quadrupole splitting, which has shown to be positive for the $(d_{xy})^2(d_{xz},d_{yz})^3$ electronic ground state[7,9] and negative for the $(d_{xz},d_{yz})^4(d_{xy})^1$ electronic ground state.[17]

NMR spectroscopy is useful for differentiating the two electronic ground states at ambient temperatures, where the $(d_{xy})^2(d_{xz},d_{yz})^3$ ground state exhibits pyrrole-H resonances at negative chemical shifts (-12 to -30 ppm, depending on axial ligands and temperature),[24] while the $(d_{xz},d_{yz})^4(d_{xy})^1$ ground state exhibits pyrrole-H resonances in the diamagnetic region of the NMR spectrum (0 to $+10$ ppm).[25−29] It is also often possible to determine the energy separation of the two electronic states from the curvature of the Curie plot.[30] Some time ago, La Mar and co-workers[31,32] recognized that the hyperfine shifts for both the pyridine ligands and the tetraphenylporphyrin of a series of $[(TPP)Fe(R\text{-}Py)_2]^+$ are very sensitive to the basicity of the axial ligands. More recently, Safo et al.[33] reported similar trends in hyperfine shifts for tetramesitylporphinatoiron(III) bis(pyridine) complexes as a function of ligand basicity, and Simonneaux and co-workers reported that when two molecules of *tert*-butyl isocyanide are bound to ferric tetraphenylporphyrin, the ^{1}H NMR spectrum is indicative of a low-spin complex,[26,34] but with isotropic shifts very different than those of any low-spin Fe(III) porphyrinate reported previous to that time. The hyperfine shifts were found to reflect the very small magnetic anisotropy of the iron, and an unusual pattern of unpaired spin density when nitrogen donor axial ligands are exchanged for isocyanide ligands, with a completely reversed pattern of delocalization.[26] Subsequently, it was recognized that the unusual ^{1}H NMR behavior results from the existence of the $(d_{xz},d_{yz})^4(d_{xy})^1$ ground state.[11] Similar NMR results were later obtained for octaethylporphinatoiron(III) bis(*tert*-butyl isocyanide), where it could readily be seen that there is very large π spin density at the *meso* positions of the porphyrinate ring.[17] This, combined with the extremely small amount of spin density present at the pyrrole positions of both the TPP[26] and OEP[17] analogues, indicates that there is significant spin delocalization to the $a_{2u}(\pi)$ orbital, which is possible only if the porphyrinate ring is highly ruffled, causing twisting of the nitrogen p_z orbitals from the normal to the porphyrin ring.[11,17,25]

Although isocyanides are not natural substrates in biological systems, their interactions with heme proteins have been studied extensively. Thus, the reaction between protoheme and methyl isocyanide was first reported by Warburg et al. in 1929.[35] The purpose was to study the effects of methyl isocyanide on the photochemical dissociation of CO-hemoglobin. The formation of the isocyanide−hemoglobin complex was later described more thoroughly by Keilin,[36] St. George and Pauling,[37] and Antonini and Brunori.[38] Indeed, the idea that interactions with protein residues control the binding of ligands to hemoglobin was first recognized by St. George and Pauling[37] using isocyanide binding with increasing steric bulk of the alkyl group. More recent approaches have been developed by Olson, Gibson, and

(8) Hatano, K.; Safo, M. K.; Walker, F. A.; Scheidt, W. R. *Inorg. Chem.* **1991**, *30*, 1643.
(9) Safo, M. K.; Gupta, G. P.; Walker, F. A.; Scheidt, W. R. *J. Am. Chem. Soc.* **1991**, *113*, 5497.
(10) Munro, O. Q.; Serth-Guzzo, J. A.; Turowska-Tyrk, I.; Mohanrao, K.; Walker, F. A.; Debrunner, P. G.; Scheidt, W. R. *J. Am. Chem. Soc.* **1999**, *121*, 11144.
(11) Safo, M. K.; Walker, F. A.; Raitsimring, A. M.; Walters, W. P.; Dolata, D. P.; Debrunner, P. G.; Scheidt, W. R. *J. Am. Chem. Soc.* **1994**, *116*, 7760.
(12) Cheesman, M. R.; Walker, F. A. *J. Am. Chem. Soc.* **1996**, *118*, 7373.
(13) Bracete, A. M.; Kadkhodayan, S.; Sono, M.; Huff, A. M.; Zhuang, C.; Cooper, D. K.; Smith, K. M.; Chang; C. K.; Dawson, J. H. *Inorg. Chem.* **1994**, *33*, 5042.
(14) Peng, Q.; Timkovich, R.; Loewen, P. C.; Peterson, J. *FEBS Lett.* **1992**, *309*, 157.
(15) Coulter, E. D.; Sono, M.; Chang, C. K.; Lopez, O.; Dawson, J. H. *Inorg. Chim. Acta* **1995**, *240*, 603.
(16) Sutherland, J.; Greenwood, C.; Peterson, J.; Thomson, A. J. *Biochem. J.* **1986**, *233*, 893.
(17) Walker, F. A.; Nasri, H.; Turowska-Tyrk, I.; Mohanrao, K.; Watson, C. T., Shokhirev, N., V.; Debrunner, P. G.; Scheidt, W. R. *J. Am. Chem. Soc.* **1996**, *118*, 12109.
(18) Chiu, J. T.; Loewen, P. C.; Switala, J.; Gennis, R. B.; Timkovich, R. *J. Am. Chem. Soc.* **1989**, *111*, 7046.
(19) Lorence, R. M.; Gennis, R. B. *J. Biol. Chem.* **1989**, *264*, 7135.
(20) Chang, C. K.; Wu, W. *J. Biol. Chem.* **1986**, *261*, 8593.
(21) Crane, B. R.; Siegel, L. M.; Getzoff, E. D. *Science* **1995**, *270*, 59.
(22) Griffith, J. S. *Proc. R. Soc. London, A* **1956**, *235*, 23.
(23) Taylor, C. P. S. *Biochim. Biophys. Acta* **1977**, *491*, 137.
(24) La Mar, G. N.; Walker, F. A. In *The Porphyrins*; Dolphin, D., Ed.; Academic Press: New York, 1979; pp 61−157.
(25) Walker, F. A.; Simonis, U. In *Biological Magnetic Resonance*; Berliner, L. E., Reuben, J., Ed.; Plenum: NY, 1993; Vol. 12, p 132 and references therein.
(26) Simonneaux, G.; Hindré, F.; Le Plouzennec, M. *Inorg. Chem.* **1989**, *28*, 823.
(27) Nakamura, M.; Ikeue, T.; Fujii, H.; Yoshimura, T. *J. Am. Chem. Soc.* **1997**, *119*, 6284.
(28) Nakamura, M.; Ikeue, T.; Fujii, H.; Yoshimura, T.; Tajima, K. *Inorg. Chem.* **1998**, *37*, 7, 2405.
(29) Walker, F. A. In *The Porphyrin Handbook*; Kadish, K. M., Smith, K. M., Guilard, R., Eds.; Academic Press: San Diego, CA, 2000; Vol. 5, Chapter 36, pp 81−183.
(30) Shokhirev, N. V.; Walker, F. A. *J. Phys. Chem.* **1995**, *99*, 17795.
(31) La Mar, G. N.; Bold, T. J.; Satterlee, J. D. *Biochim. Biophys. Acta* **1977**, *498*, 189.
(32) La Mar, G. N.; del Gaudio, J.; Frye, J. S. *Biochim. Biophys. Acta* **1977**, *498*, 422.
(33) Safo, M. K.; Gupta, G. P.; Watson, C. T.; Simonis, U.; Walker, F. A.; Scheidt, W. R. *J. Am. Chem. Soc.* **1992**, *114*, 7066.
(34) Geze, C.; Legrand, N.; Bondon, A.; Simonneaux, G. *Inorg. Chim. Acta* **1992**, *195*, 73.
(35) Warburg, O.; Negelein, E.; Christian, W. *Biochem. Z.* **1929**, *214*, 26.
(36) Keilin, J. *Biochem. J.* **1949**, *45*, 440.
(37) St. George, R.; Pauling, L. *Science* **1951**, *114*, 629.
(38) Antonini, E.; Brunori, M. In *Hemoglobin and Myoglobin in their Reactions with Ligands*; North-Holland Pub. Co.: Amsterdam, 1971; p 34.

others.[39−52] Elegant studies of the structure−reactivity relationships in myoglobin have been developed by assessing the effects of substitution in the heme cavity using site-directed mutagenesis.[45] In these studies, various alkyl isocyanides were tested, along with more classical ligands such as dioxygen and carbon monoxide. The large size of the alkyl isocyanide ligand was used to amplify the effects of the mutation.

Extensive thermodynamic and kinetic studies of alkyl isocyanide complexation to hemoglobin, myoglobin,[38−45] and other heme proteins[53−55] have been reported, but many questions still remain. First, despite the accuracy of these methods, conflicting results persist with regard to the binding of aryl isocyanides to myoglobin.[56,57] Thus, the intrinsic electronic effect on ligand binding associated with differences between alkyl and aryl isocyanides is still under debate. Second, the reason complexation of isocyanides with the ferric state is possible with cytochromes P450, whereas no ligation is observed with myoglobin and hemoglobin, is still not clear. Consequently, studies of the reactions of isocyanides with simple synthetic iron(III) porphyrinates,[58−62] which have been more limited, deserve special attention.

We have found in this study that Mössbauer spectroscopy is extremely informative concerning the effects of the electronic structure of the low-spin Fe(III) center on the bonding interactions with the ligands, as well as the nature of the ground and excited states and an estimation of the energy separation between them. This spectroscopic technique measures the nuclear energy levels as they are perturbed by external fields and hyperfine interactions. The magnetic hyperfine interaction couples the nuclear spin I to the electron spin S, and transitions among the electronic eigenstates $m_s = +1/2$ and $m_s = -1/2$ lead to fluctuations in the nuclear Hamiltonian. In most cases, magnetic Mössbauer spectra are analyzed either in the slow or the fast relaxation limit. In the limit of slow spin relaxation (fluctuation), typically at temperatures around 4.2 K, the Mössbauer spectra may be calculated by assuming the electronic Hamiltonian $\hat{H}_e$ to be stationary and the two Zeeman levels to be populated according to the Boltzmann factor. At higher temperatures the fast fluctuation limit applies, and a thermal average of the spin expectation value $\langle S \rangle$ can be substituted into the nuclear Hamiltonian. This is applicable for the case of spin lattice relaxation typically at temperatures above 150 K, or for fast spin−spin relaxation, the latter being often observed in powder samples. For the case of intermediate relaxation, the resulting changes in the energy spectrum of the Mössbauer transitions are observable if the Larmor frequency of the iron nucleus ω_L is comparable to the spin transition rate w but large compared to the nuclear decay rate, $1/\tau = 7 \times 10^6\ s^{-1}$.[63] In this study we show that the complexes tetra(*p*-tolyl)porphyrinatoiron(III) bis-(2,6-xylyl isocyanide) trifluoromethylsulfonate (**1**), tetraphenylporphyrinatoiron(III) bis(2,6-xylyl isocyanide) trifluoromethylsulfonate (**2**), and tetra(*m*-tolyl)porphyrinatoiron(III) bis(2,6-xylyl isocyanide) trifluoromethylsulfonate (**3**) possess the $(d_{xz},d_{yz})^4(d_{xy})^1$ electronic ground state. We also demonstrate that the Mössbauer spectra of these three complexes, even at magnetic fields up to 5.35 T at 4.2 K, are influenced by electronic spin−spin relaxation in the intermediate relaxation regime. We have analyzed the Mössbauer spectra by using the dynamic line shape formalism of Blume and Clauser.[64] This method has been applied previously to spin fluctuation rates of high-spin ferrous rubredoxin[63] and to catalytic intermediates of horseradish peroxidase,[65] cytochrome $P450_{CAM}$, protocatechuate dioxygenase, and horseradish peroxidase compounds I and II.[66] Magnetic Mössbauer spectra of low-spin ferric hemes have been analyzed in terms of either fast or slow relaxation limits in the past.[7,9,17] To our knowledge, this work is the first which studies the influence of electron spin fluctuations on the Mössbauer spectra of low-spin ferric heme compounds, either models or proteins. The reasons these particular complexes should be in the intermediate spin fluctuation regime and the likelihood of observing this phenomenon in a heme protein are discussed.

Experimental Section

General Information. As a precaution against the formation of the μ-oxo dimer $[Fe(TPP)]_2O$,[67] all reactions were carried out in dried solvents in Schlenk tubes under an argon atmosphere. Solvents were distilled from appropriate drying agents and stored under argon. ^1H NMR spectra were recorded on a Bruker AC 300P spectrometer in $CDCl_3$ at 300 MHz. Tetramethylsilane was used as internal reference. Temperatures are given to within 1 K. Visible spectra were measured on a Uvikon 941 spectrometer in CH_2Cl_2. Infrared spectra were recorded on a Nicolet 205 FTIR instrument in CH_2Cl_2 solution. Elemental analyses were performed by the Service Central of Analyses (CNRS) at Vernaison, France. EPR spectra were recorded on a conventional X-band spectrometer (Bruker 200D SRC) equipped with a He flow cryostat (ESR 910, Oxford Instruments). Spectra were taken at 10 K

(39) For fast kinetics studies of myoglobin, see for example refs 40−52.

(40) Gibson, Q. H.; Olson, J. S.; McKinnie, R. E.; Rohlfs, R. J. *J. Biol. Chem.* **1986**, *261*, 10228.

(41) Olson, J. S.; Rohlfs, R. J.; Gibson, Q. H. *J. Biol. Chem.* **1987**, *262*, 12930.

(42) Belleli, A.; Blackmore, R. S.; Gibson, Q. H. *J. Biol. Chem.* **1990**, *265*, 13595.

(43) Jongeward, K. A.; Magde, D.; Taube, D. J.; Marsters, J. C.; Traylor, T. G.; Sharma, V. S. *J. Am. Chem. Soc.* **1988**, *110*, 380.

(44) Wood, M. A.; Dickinson, K.; Willey, G. R.; Dodd, G. H. *Biochem. J.* **1987**, *247*, 675.

(45) Olson, J. S.; Mathews, A. J.; Rohlfs, R. J.; Springer, B. A.; Egeberg, K. D.; Sligar, S. G.; Tame, J.; Renaud, J. P.; Nagai, K. *Nature* **1988**, *336*, 265.

(46) Mathews, A. J.; Rohlfs, R. J.; Olson, J. S.; Tame, J.; Renaud, J. P.; Nagai, K. *J. Biol. Chem.* **1989**, *264*, 16573.

(47) Rohlfs, R. J.; Mathews, A. J.; Carver, T. E.; Olson, J. S.; Springer, B. A.; Egeberg, K. D.; Sligar, S. G. *J. Biol. Chem.* **1990**, *265*, 3168.

(48) Egeberg, K. D.; Springer, B. A.; Sligar, S. G.; Carver, T. E.; Rohlfs, R. J.; Olson, J. S. *J. Biol. Chem.* **1990**, *265*, 11788.

(49) Carver, T. E.; Olson, J. S.; Smerdon, S. J.; Krzywda, S.; Wilkinson, A. J.; Gibson, Q. H.; Blackmore, R. S.; Ropp, J. D.; Sliger, S. G. *Biochemistry* **1991**, *30*, 4697.

(50) Smerdon, S. J.; Dodson, G. G.; Wilkinson, A. J.; Gibson, Q. H.; Blackmore, R. S.; Carver, T. E.; Olson, J. S. *Biochemistry* **1991**, *30*, 6252.

(51) Carver, T. E.; Brantley, R. E.; Singleton, E. W.; Arduini, R. M.; Quillin, M. L.; Phillips, G. N.; Olson, J. S. *J. Biol. Chem.* **1992**, *267*, 14443.

(52) Smerdon, S. J.; Krzywda, S.; Wilkinson, A. J.; Brantley, R. E.; Carver, T. E.; Hargrove, M. S. Olson, J. S. *Biochemistry* **1993**, *32*, 5132.

(53) White, R. E.; Coon, M. J. *J. Biol. Chem.* **1982**, *257*, 3073.

(54) Sono, M.; Dawson, J. H.; Hall, K.; Hager, L. P. *Biochemistry* **1986**, *25*, 347.

(55) Imai, Y.; Okamoto, N.; Nakahara, K.; Shoun, H. *Biochim. Biophys. Acta* **1997**, *1337*, 66.

(56) Caughey, W. S.; Barlow, C. H.; O'Keeffe, D. H.; O'Toole, M. C. *Ann. N.Y. Acad. Sci.* **1973**, *206*, 296−309.

(57) Patel, M. J.; Kassner, R. J. *Biochem. J.* **1989**, *262*, 959.

(58) For ferrous porphyrinate isocyanide derivatives, see for example refs 59−61.

(59) Caughey, W. S.; Barlow, C. H.; O'Keeffe, D. H.; O'Toole, M. C. *Ann. N.Y. Acad. Sci.* **1973**, *206*, 296.

(60) Jameson, G. B.; Ibers, J. A. *Inorg. Chem.* **1979**, *18*, 1200.

(61) Le Plouzennec, M.; Bondon, A.; Sodano, P.; Simonneaux, G. *Inorg. Chem.* **1986**, *25*, 1254.

(62) For ferric porphyrin isocyanide derivatives, see for example refs 17, 26, and 34.

(63) Winkler, H.; Schulz, C.; Debrunner, P. G. *Phys. Lett.* **1979**, *69A*, 360.

(64) Clauser, M. J.; Blume, M. *Phys. Rev. B* **1971**, *3*, 583.

(65) Schulz, C. E.; Rutter, R.; Sage, J.P.; Debrunner, P. G.; Hager, L. P. *Biochemistry* **1984**, *23*, 4743.

(66) Schulz, C. E.; Nyman, P.; Debrunner, P. G. *J. Chem. Phys.* **1987**, *87*. 5076.

(67) Fleischer, E. B.; Palmer, J. M.; Srivastava, T. S.; Chatterjee, A. *J. Am. Chem. Soc.* **1971**, *93*, 3162.

and a microwave power of 20 μW, a modulation frequency of 100 kHz, and a modulation amplitude of 5 G. Mössbauer spectra were recorded using a conventional spectrometer in the constant acceleration mode. Isomer shifts are given relative to α-Fe at room temperature. The spectra obtained at 20 mT were measured in a He bath cryostat (Oxford MD 306) equipped with a pair of permanent magnets. Spectra obtained at 1 T were measured in an in-house-made bath cryostat equipped with a superconducting magnet. For the high-field spectra (5.35 T), a cryostat also equipped with a superconducting magnet (Oxford Instruments) was used. Magnetically split spectra of paramagnetic samples were simulated in the spin-Hamiltonian approximation described below.

Reagents. The following iron porphyrins[68] were prepared by literature methods: [(TPP)FeCF$_3$SO$_3$],[69] [(*p*-TTP)FeCF$_3$SO$_3$],[70] and [(*m*-TTP)FeCF$_3$SO$_3$].[70] The 2,6-xylyl isocyanide (2,6-xylylNC) was obtained from Fluka. Aromatic isocyanides are probably not very strong coordinating ligands for the ferric state due to a decrease of basicity of the ligand in comparison to that of alkyl isocyanides,[71,72] thus making iron(III) complexation more difficult. Using triflate, a weak axial ligand,[69,70] as an intermediate permits solving this problem.

Syntheses. [(*p*-TTP)Fe(2,6-xylylNC)$_2$]CF$_3$SO$_3$ (1). To a solution of 0.2 g (0.23 mmol) of [(*p*-TTP)FeCF$_3$SO$_3$] in 10 mL of dichloromethane was added 8 equiv 2,6-xylylNC in 2 mL by a syringe while the solution was stirred at room temperature. Then 40 mL of hexane and 1 mL of toluene were added, and the solution was set aside for 2 days for crystallization at 25 °C. Purple crystals of **1** were collected by filtration and washed with hexane. The yield was 0.22 g (85%). UV−vis (toluene): λ_{max}/nm 417 (ϵ 118 mM^{-1} cm^{-1}), 505 (ϵ 12), 569 (ϵ 8).

[(TPP)Fe(2,6-xylylNC)$_2$]CF$_3$SO$_3$ (2). To a solution of 0.20 g (0.23 mmol) of [(TPP)Fe]CF$_3$SO$_3$ in 16 mL of dichloromethane was added 8 equiv of the ligand by syringe with stirring at room temperature. Then 60 mL of pentane was added, and the solution was set aside for 2 days for crystallization at 0 °C. Purple crystals of **2** were collected by filtration and washed with hexane. The yield was 0.20 g (72%). Anal. Calcd for $C_{63}H_{46}N_6O_3F_3SFe$: C, 70.06; H, 4.26; N, 7.78. Found: C, 70.08; H, 4.56; N, 7.65. UV−vis (toluene): λ_{max}/nm 418 (ϵ 120 mM^{-1} cm^{-1}), 505 (ϵ 11), 569 (ϵ 8).

For the preparation of the *m*-tolyl derivative, [(*m*-TTP)Fe(2,6-xylylNC)$_2$]CF$_3$SO$_3$ (**3**), the same procedure was used with the corresponding triflate analogue in dichloromethane solvent and the ligand. However, for the *m*-tolyl derivative, a partial decomposition was observed; the solutions were reduced in volume to ensure precipitation, due to the high solubility of the *m*-tolyl derivative in dichloromethane. Data for [(*m*-TTP)Fe(2,6-xylylNC)$_2$]CF$_3$SO$_3$ follow. Yield: 78%. UV−vis (toluene): λ_{max}/nm 417 (ϵ 120 mM^{-1} cm^{-1}), 505 (ϵ 12), 569 (ϵ 7).

X-ray Structure Determination. The X-ray study was carried out on an Enraf-Nonius CAD-4 diffractometer using graphite-monochromatized Mo Kα radiation. The cell parameters were obtained by fitting a set of 25 high-θ reflections. Crystallographic data are collected in Table 1. Crystals of the compound were obtained as reported above. Atomic scattering factors were taken from the *International Tables for X-ray Crystallography*. All calculations were performed on a Silicon Graphics Indy computer with the Molen package[73] for refinement and ORTEP calculations.

Single-Crystal Structure Determination on [(*p*-TTP)Fe(2,6-xylylNC)$_2$]CF$_3$SO$_3$ (1). The data collection ($2\theta_{max} = 54°$, scan $\omega/2\theta = 1$, $t_{max} = 60$ s, *h,k,l* range $h = 0.14$, $k = 0.38$, $l = -23.23$, intensity controls without appreciable decay (0.15%)) gave 14 105 reflections from which 3613 reflections satisfied $I > 3\sigma(I)$. After Lorentz and polarization corrections the structure was solved by direct methods,[74] which revealed the non-hydrogen atoms of the cation and the anion. After scale factor calculations and difference Fourier, several peaks were found and assigned to the nonstoichiometric dichloromethane and toluene. After anisotropic refinement, all the hydrogen atoms of the cation moiety were found with a Fourier difference map. The whole structure was refined by the full-matrix least-squares techniques (use of *F* magnitude; *x, y, z,* $\beta_{i,j}$ for Fe, N, and C atoms; *x, y, z,* and *B* for triflate anion; and *x, y, z* for hydrogen atoms; 780 variables and 3613 observations; $w = 1/\sigma(F_o)^2 = [\sigma^2(I) + (0.04F_o^2)^2]^{-1/2}$) with the resulting $R = 0.075$, $R_w = 0.080$, and $S_w = 2.95$ (residual $\Delta\rho < 0.45$ e Å^{-3}).

Table 1. Crystallographic Data for [(*p*-TTP)Fe(2,6-xylylNC)$_2$]CF$_3$SO$_3$ (**1**)

compound	**1**·$^1/_2$(CH$_2$Cl$_2$)
empirical formula	$C_{67}H_{54}FeF_3N_6O_3S$, 1/2(CH$_2$Cl$_2$)
FW	1259.19
crystal system	monoclinic
space group	$P2_1/c$
a, Å	11.330(2)
b, Å	30.343(7)
c, Å	18.096(9)
β, deg	102.34(3)
V, Å^3	6077(5)
Z	4
P_{calc}, g·cm^{-3}	1.376
μ, cm^{-1}	4.295
T, K)	294
R_w	0.080
final *R*	0.075

Mössbauer Theory and Spectral Analysis. (a) Spin-Hamiltonian Formalism. The Zeeman interaction of a spin $\vec{S}$ with an applied field $\vec{B}$, with $\bar{\bar{g}}$ representing the electronic $\bar{\bar{g}}$-tensor, is described by the Hamiltonian

$$\hat{H}_{eff} = \mu_B \vec{S}\bar{\bar{g}}\vec{B} \tag{1}$$

where μ_B denotes the Bohr magneton.

Magnetic Mössbauer spectra were simulated using eq 1 to derive the spin-expectation $\langle S \rangle$ together with the nuclear Hamiltonian,[75,76]

$$\hat{H}_N = \frac{eQV_{zz}}{4I(2I-1)}[3\hat{I}_z^2 - I(I+1) + \eta(\hat{I}_x^2 - \hat{I}_y^2)] - g_N\mu_N\vec{I}\vec{B} + \langle\vec{S}\rangle\bar{\bar{A}}\vec{I} \tag{2}$$

Here, *I* denotes the nuclear spin-quantum number of the ground and excited nuclear states, *Q* the nuclear quadrupole moment of the excited nuclear state, V_{zz} the main component of the electric field gradient (efg) tensor, $\eta = (V_{xx} - V_{yy})/V_{zz}$ the asymmetry parameter of the efg, and g_N the nuclear *g*-factor of the ground and excited statez. $\bar{\bar{A}}$ is the hyperfine coupling tensor.

(b) Analysis of Mössbauer Spectra in the Presence of Electronic Relaxation. If spin−lattice relaxation is the dominant process, Mössbauer spectra are analyzed in general for two limiting cases. In the limit of slow spin fluctuation, typically at temperatures around 4.2 K, the Mössbauer spectra may be calculated by assuming $\hat{H}_e$ to be stationary and the two Zeeman levels to be populated according to the Boltzmann factor. At higher temperatures the fast fluctuation limit applies and a thermal average of the spin expectation value $\langle\vec{S}\rangle$ can be substituted in eq 2. However, if Mössbauer spectra are influenced by intermediate spin fluctuation rates caused by temperature-independent spin−spin relaxation, neither fast nor slow relaxation limits may apply. Such samples then exhibit Mössbauer spectra in the intermediate relaxation regime where the nuclear Larmor frequency is comparable to the spin transition rate over the whole experimentally accessible

(68) Abbreviations used: H_2TPP, tetraphenylporphyrin; H_2(*m*-TTP), tetrakis(*m*-tolyl)porphyrin; H_2(*p*-TTP), tetrakis(*p*-tolyl)porphyrin; (2,6-xylylNC), 2,6-xylyl isocyanide.

(69) Reed, C. A.; Mashiko, T.; Bentley, S. P.; Kasner, M. E.; Scheidt, W. R.; Spartalian, K.; Lang, G. *J. Am. Chem. Soc.* **1979**, *101*, 2948.

(70) Goff, H.; Shimomura, E. *J. Am. Chem. Soc.* **1980**, *102*, 31.

(71) Malatesta, L.; Bonati, F. *Isocyanide Complexes of Metals*; Wiley (Interscience): New York, 1969.

(72) Singleton, E.; Oosthuizen, E. *Adv. Organomet. Chem.* **1983**, *22*, 209.

(73) ENRAF−NONIUS Molecular Determination Package, Delft University, The Netherlands, 1990.

(74) Sheldrick, G. M. In *Crystallographic Computing 3: Data Collection, Structure Determination, Proteins and Databases*; Sheldrick, G. M., Krüger, C., Goddard, R., Eds; Clarendon Press: Oxford, 1985.

(75) Wickman, H. H.; Klein, M. P.; Shirley, D. A. *Phys. Rev.* **1966**, *152*, 345.

(76) Trautwein, A. X.; Bill, E.; Bominaar, E. L.; Winkler, H. *Struct. Bonding* **1991**, *78*, 1.

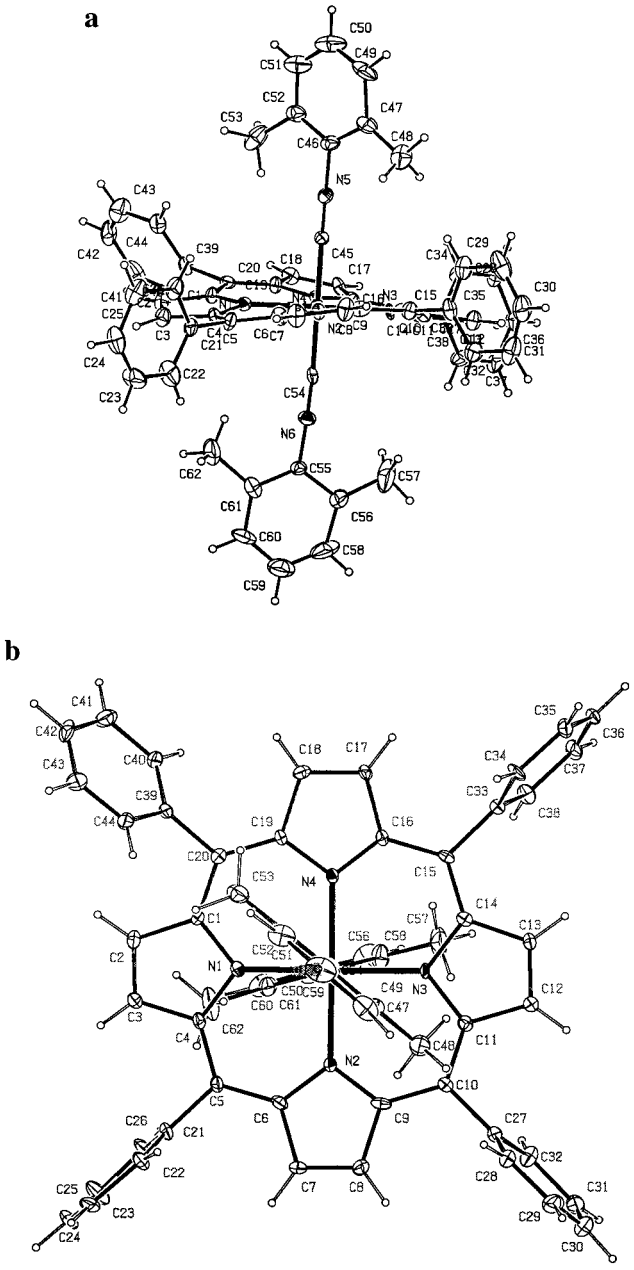

Figure 1. ORTEP diagram of [(*p*-TTP)Fe(2,6-xylylNC)$_2$]CF_3SO_3 (**1**) (a) looking at the complex along the mean plane of the porphyrin and (b) looking down on the porphyrin ring. Labels assigned to the crystallographically unique atoms are displayed. Atoms are contoured at the 50% probability level.

temperature range. The ferric low-spin samples discussed in this work exhibit such spectra. The case of intermediate spin fluctuation is treated by using the dynamic line shape formalism of Blume and Clauser,[64] which has been elaborated by Winkler et al.[63]

Results and Discussion

Structure Determination. The molecular structure of the cation of [(*p*-TTP)Fe(2,6-xylylNC)$_2$]CF_3SO_3 (**1**) is shown in the ORTEP diagrams of Figure 1a and 1b (and of the complete molecular unit in Figure S1 in the Supporting Information), along with the numbering scheme for the crystallographically unique atoms. As shown in Figure 1b, the xylyl rings of the axial ligands are not in parallel planes. The dihedral angles between the planes of the individual xylyl groups and the N_1,N_3 axis are 39.6(2) and 15.5(2)°, yielding a dihedral angle between the planes of the two xylyl groups of 55.1°. The dihedral angles between the porphyrinate plane and the planes of the four phenyl rings are 119.4(3), 67.7(3), 108.9(3), and 66.1(3)° for **1**; these values are well removed from 90° but are not unusual.

Table 2. Selected Bond Distances (Å) and Bond Angles (deg) for [(*p*-TTP)Fe(2,6-xylylNC)$_2$]CF_3SO_3 (**1**)[a]

	Distances		
Fe−N(1)	1.937(7)	Fe−C(49)	1.95(1)
Fe−N(2)	1.965(7)	Fe−C(58)	1.92(2)
Fe−N(3)	1.967(7)	C(49)−N(5)	1.13(1)
Fe−N(4)	1.974(7)	C58−N(6)	1.16(1)
	Angles		
N(1)−Fe−N(2)	89.9(4)	C(49)−Fe−N(3)	86.5(4)
N(1)−Fe−N(3)	179.4(4)	C(49)−Fe−N(4)	92.2(4)
N(1)−Fe−N(4)	89.6(4)	C(58)−Fe−N(1)	93.5(4)
N(2)−Fe−N(3)	90.4(4)	C(58)−Fe−N(2)	91.9(4)
N(2)−Fe−N(4)	179.4(4)	C(58)−Fe−N(3)	86.0(4)
N(3)−Fe−N(4)	90.1(4)	C(58)−Fe−N(4)	87.8(4)
C(49)−Fe−N(1)	94.0(4)	Fe−C(49)−N(5)	172.8(9)
C(49)−Fe−N(2)	88.1(4)	Fe−C(58)−N(6)	172.8(9)
C(49)−Fe−C(58)	172.5(4)		

[a] Standard deviations in parentheses.

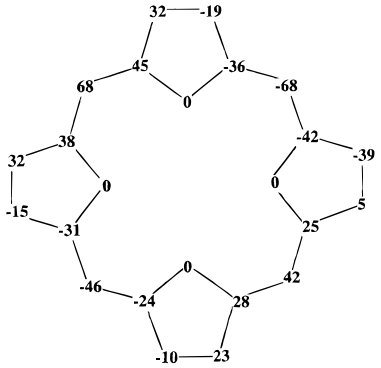

Figure 2. Formal diagram of the porphyrinato core in [(*p*-TTP)Fe(2,6-xylylNC)$_2$]CF_3SO_3 (**1**) showing deviations of each unique atom from the mean plane of the core (units 0.01 pm).

Selected individual bond distances and angles for [(*p*-TTP)Fe(2,6-xylylNC)$_2$]CF_3SO_3 (**1**) are given in Table 2, and the complete lists of distances and angles are given in Tables S1 and S2 (Supporting Information), respectively. Positional parameters and general displacement parameters, *B*, are given in Tables S3 and S4 (Supporting Information), respectively. The metal−carbon bond distances of the isocyanide ligands average to 1.935(10) Å for **1** and are slightly longer than those observed in the analogous iron(III) complex containing *tert*-butyl isocyanide ligands (1.915 (20) Å).[17] This is consistent with the greater σ donor ability of alkyl isocyanide ligands compared with that of aryl isocyanides and with a concomitant increase in σ bonding from the axial ligand to iron.

The equatorial Fe−N bond distances average to 1.961(6) Å for **1**, which is quite short for low-spin iron(III) porphyrinate derivatives.[77,78] These short distances are consistent with the significant ruffling of the porphyrinate core, which is very similar to that recently reported in perchlorato derivatives of bis(4-cyanopyridine)tetraphenylporphyrinatoiron(III)[11,33] and of bis(*tert*-butyl isocyanide) octaethyl- and tetraphenylporphyrinatoiron(III).[17] Deviation of each unique atom from the mean plane of the core of **1** is shown in Figure 2. The ruffling of the core is quite apparent in the complex and similar to the ruffling observed in bis(*tert*-butyl isocyanide) octaethyl- and tetraphe-

(77) Scheidt, W. R.; Reed, C. A. *Chem. Rev.* **1981**, *81*, 43.
(78) Scheidt, W. R.; Lee, Y. J. *Struct. Bonding (Berlin)* **1987**, *64*, 1.

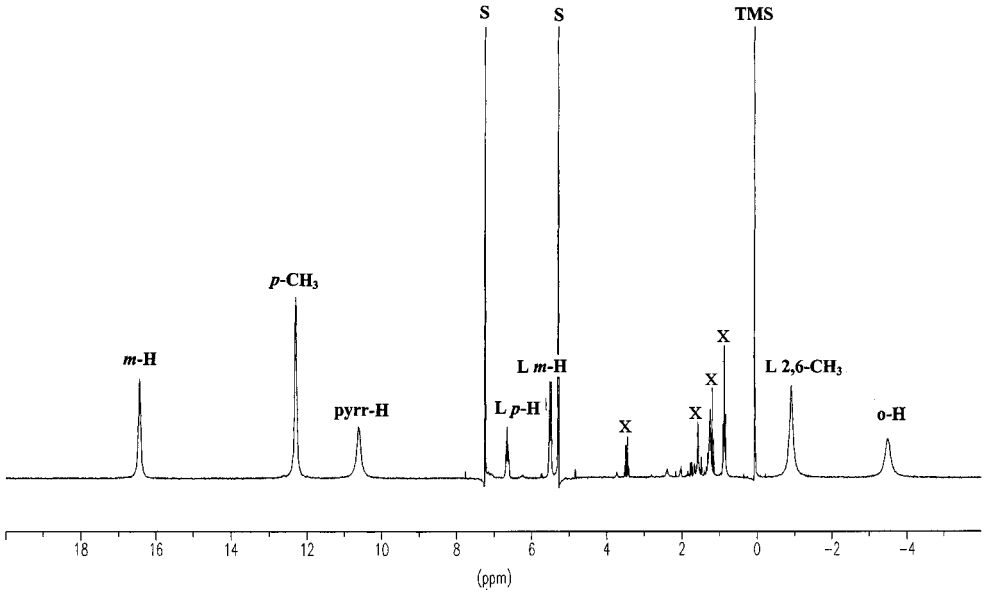

Figure 3. ^{1}H NMR spectrum of [(*p*-TTP)Fe(2,6-xylylNC)$_2$]CF$_3$SO$_3$ (**1**) recorded at 297 K in CDCl$_3$. Assignments of the various resonances are indicated; S marks the residual solvent peaks (chloroform and dichloromethane), and x marks minor impurities.

nylporphyrinatoiron(III)[17] and [(4-CN-Py)$_2$Fe(TPP)]ClO$_4$.[11] The 55.1° dihedral angle between xylyl planes mentioned above is apparently not related to the ruffling of the porphyrin ring, and hence the observed angle may arise from crystal packing considerations. A packing diagram is shown in Figure S2 (Supporting Information).

IR Spectroscopy. Determination of the isocyanide stretching frequencies in heme isocyanides provides an opportunity to demonstrate clearly the sensitivity of ligand binding to the electronic properties of the second axial ligand and the metalloporphyrin. For example, the ν(CN) stretching frequency of CNR is increased upon coordination of the aromatic isocyanide to iron(III) porphyrin from 2135 cm^{-1} for the free ligand to 2195 cm^{-1} in [(*p*-TTP)Fe(2,6-xylylNC)$_2$]CF$_3$SO$_3$ (**1**). This increase of the stretching frequency, which indicates a higher bond order in the complex than in the free ligand, is consistent with the formal positive charge on the iron.[71] However, the data suggest that the observed isocyanide stretching frequencies upon complexation are also influenced by the electronic nature of the phenyl group on the isocyanide ligand. As expected, the ν(CN) stretching frequency of ligated 2,6-xylylisocyanide is lower than that of ligated *t*-BuNC upon coordination of the isocyanide to [(*p*-TTP)FeCF$_3$SO$_3$]; ν(NC) increases from 2195 cm^{-1} for **1** to 2220 cm^{-1} in [(TPP)Fe(*t*-BuNC)$_2$]CF$_3$SO$_3$ ($\Delta\nu$ = 25 cm^{-1}).[17] This is consistent either with a greater π-acceptor ability of the aryl isocyanide ligand as compared with that of the alkyl isocyanide ligand and with a concomitant increase in π back-bonding from iron to the CN bond, or with a weaker σ-donating ability of the aromatic isocyanide ligand relative to that of the alkyl isocyanide ligand.

NMR Spectroscopy. The ^{1}H NMR spectrum of [(*p*-TTP)-Fe(2,6-xylylNC)$_2$]CF$_3$SO$_3$ (**1**) at 297 K is shown in Figure 3. The isotropic shifts are listed in Table 3. The peaks for the phenyl protons of the porphyrin ring are assigned completely by methyl substitution in combination with 1D proton NMR decoupling experiments (not shown). For the isocyanide ligands, the relative intensities determine the assignment. The shifts of the isocyanide ligand are independent of the presence of excess ligand, and hence axial ligand dissociation does not appear to be significant at ambient temperature. The spectrum of [(*p*-TTP)-Fe(2,6-xylylNC)$_2$]CF$_3$SO$_3$ (**1**) shows the pyrrole proton signal at a downfield position, 10.7 ppm, as compared to 9.7 ppm for [(TPP)Fe(*t*-BuNC)$_2$]CF$_3$SO$_3$.[26] This contrasts with the pyrrole proton signals of most other low-spin Fe(III) porphyrinates at ambient temperature, including [(TPP)Fe(N-MeIm)$_2$]ClO$_4$ (δ = −17 ppm)[25] and [(TPP)Fe(P(Me)$_2$Ph)$_2$]ClO$_4$ (δ = −19.4 ppm),[79] and provides confirmation of the $(d_{xz},d_{yz})^4(d_{xy})^1$ electronic structure in these aryl isocyanide derivatives. Magnetic measurements using the method of Evans[80,81] were made for 0.03 M CD$_2$Cl$_2$ solutions of **1** at 297 K, employing Me$_4$Si as the reference. The solution magnetic moment (μ = 1.9 μ_B) is compatible with the low-spin state, $S = {}^1/_2$.

Table 3. Observed Shifts and Separation of the Isotropic Shift into Contact and Dipolar Contributions in [(*p*-TTP)Fe(2,6-xylylNC)$_2$]CF$_3$SO$_3$ (**1**) in CDCl$_3$ at 297 K

proton type	δ_{obs}[a]	δ_{iso}[b]	δ_{dip}[c]	δ_{con}
o-H	−3.42	−11.44	0.76	−12.20
m-H	16.51	8.9	0.35	8.55
	(0.86)[d]	(−1.65)	(0.22)	(−1.87)
p-CH$_3$	12.36	9.72	0.23	9.49
	(1.1)[e]	(−6.53)	(0.31)	(−6.84)
Pyrr-H	10.69	2.49	1.48	1.01

[a] Chemical shifts in ppm. [b] Isotropic shifts with the diamagnetic complex (TPP)Fe(*t*-BuNC)$_2$ as reference.[61] [c] Calculated from the *o*-H dipolar shift of the [TPPFe(NMeIm)$_2$]$^+$ complex,[29] scaled by the ratio of the axial *g*-anisotropies of the isocyanide complexes of this study divided by that of the NMeIm complex.[29] Other dipolar shifts calculated from that of *o*-H, based on the relative geometric factors ($3\cos^2\theta - 1)/r^3$.[24,29] [d] *m*-CH$_3$ shift of [(*m*-TTP)Fe(2,6-xylylNC)$_2$]$^+$ in parentheses. [e] *p*-H shift of [(*m*-TTP)Fe(2,6-xylylNC)$_2$]$^+$ and [(TPP)Fe(2,6-xylylNC)$_2$]$^+$ in parentheses.

The temperature dependences of the isotropic shifts of the protons of **1** in CDCl$_3$ are shown in Figure 4. The isotropic shifts appear to vary almost linearly with 1/*T* over the range of measurement, but the linearly extrapolated lines do not pass through the origin at $1/T = 0$. The deviations of the intercepts are +8.5 (*o*-H), −11 (*p*-CH$_3$), −4.5 (*m*-H), and −3.5 ppm (pyrr-H). Hence, the temperature dependence of **1** was analyzed in terms of the possibility of a thermally accessible excited state.[30]

(79) Sodano, P.; Simonneaux, G. *Inorg. Chem.* **1988**, *27*, 3956.
(80) Evans, D. F. *J. Chem. Soc.* **1959**, 2003.
(81) For superconducting magnets, the revised equation must be used: Sur, S. K. *J. Magn. Reson.* **1989**, *82*, 169.

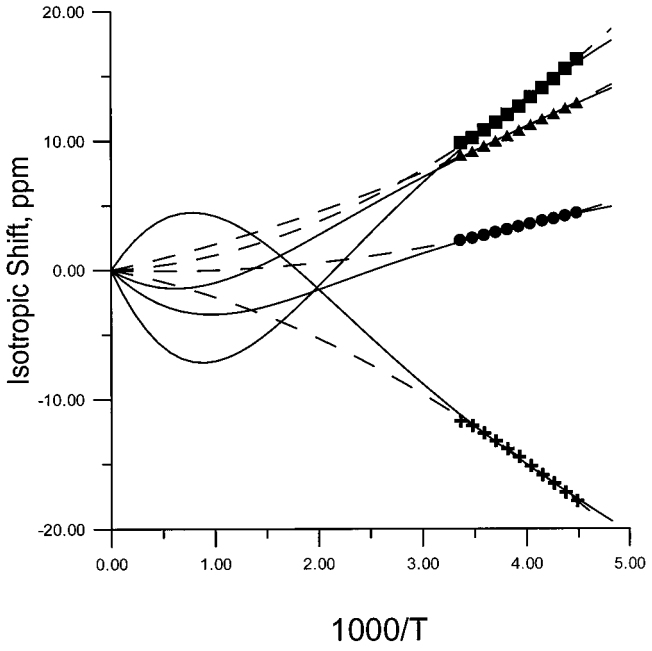

Figure 4. Curie plot of the isotropic shifts vs 1000 × reciprocal temperature (K) for [(*p*-TTP)Fe(2,6-xylylNC)$_2$]CF_3SO_3 (**1**) in $CDCl_3$, showing extended Curie law fits[30] to $\Delta E = 70$ (- - -) and 740 cm^{-1} (—). Symbols: ■, *p*-CH_3; ▲, *m*-H; ●, pyrrole-H; +, *o*-H.

This analysis showed that acceptable fits could be obtained assuming ΔE values between ground and excited states of 70 to greater than 700 cm^{-1}. Example fits for 70 and 740 cm^{-1} values of ΔE are included in Figure 4. Although the smaller ΔE value appears to fit somewhat better, the high-temperature data points may be less reliable due to the possibility of some ligand dissociation (although none was detected). As is evident from the fits shown in Figure 4, the relatively gentle temperature dependence of the experimental data down to −50 °C does not allow the determination of a unique fit. As discussed below, the temperature dependence of the quadrupole splitting, ΔE_Q, obtained from the Mössbauer data, are consistent with $\Delta E = 740$ cm^{-1}, but there may be reasons why the value of ΔE is larger in the solid state, and the process represented by this ΔE value may not be simply an excited electronic state (see below).

To characterize the iron bis-isocyanide electronic structure, the isotropic shifts were calculated for **1** by using [(TPP)Fe(*t*-BuNC)$_2$] and related *p*- and *m*-methyl substituted diamagnetic complexes as references.[61] Analysis of the isotropic shift was made according to the method of La Mar,[31] and as found for the related *tert*-butyl isocyanide complex,[26] there is a relatively large contact contribution to the *meso*-phenyl-H resonances of **1**−**3**. The mechanism of spin transfer is thus, as expected, significantly different from that observed for low-spin ferric bis-imidazole[24,25,29] and bis-phosphine[79,82] complexes of synthetic porphyrins, where the *meso*-phenyl shifts were found to be essentially completely dipolar in origin.[24,79] Using the *o*-H dipolar shift of [(TPP)Fe(N-MeIm)$_2$]$^+$ at 298 K,[24] scaled by the ratio of the axial *g*-anisotropies of the isocyanide complexes **1**−**3** divided by that of the imidazole complex,[29] the dipolar shift of the *o*-H of complexes **1**−**3** could be calculated. Then, using the relative geometric factors,[29] the dipolar contribution to the pyrrole-H and all other protons can be obtained. The resulting dipolar and contact contributions are included in Table 3. The chemical shift of the pyrrole-H resonance of complexes **1**−**3** at ambient temperatures is larger (more positive) than that for [(TPP)Fe(t-BuNC)$_2$]$^+$,[17] which leads, in Table 3, to a positive value for the contact shift of the pyrrole-H of about 1 ppm. This is not consistent with spin delocalization via porphyrin π orbitals[29] and suggests that either the dipolar shift has been underestimated or there is a small amount of σ spin delocalization to the pyrrole-H position. The latter possibility seems unlikely, because the d_{xy} orbital has nodes at the porphyrin nitrogens with respect to σ-bonding.

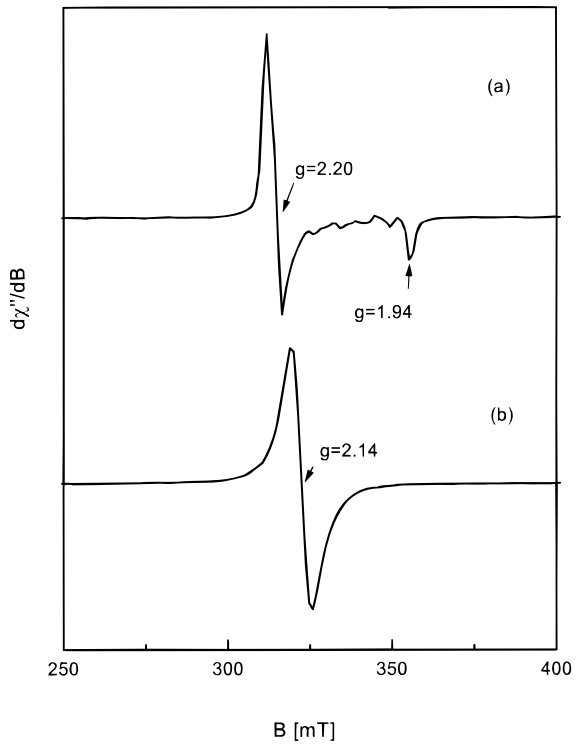

Figure 5. EPR spectrum of (a) [(*p*-TTP)Fe(2,6-xylylNC)$_2$]CF_3SO_3 (**1**) and (b) [(*m*-TTP)Fe(2,6-xylylNC)$_2$]CF_3SO_3 (**3**) in the solid state, recorded at 10 K. Experimental conditions: microwave frequency, 9.649 GHz; microwave power, 20 μW; modulation frequency, 100 kHz; modulation amplitude, 1 G.

The chemical shifts observed for the axial ligands ($\delta_{o-CH_3} = -0.85$ ppm; $\delta_{m-H} = 5.46$ ppm; $\delta_{p-H} = 6.70$ ppm) are close to those expected for groups located in the shielding region of the porphyrin ring. There should be only very small dipolar shifts for those protons because of their distance from the iron. Thus, there appears to be essentially no spin density on the axial ligands, as expected because of the orthogonality of the isocyanide p_π orbitals and the metal d_{xy} orbital that contains the unpaired electron.

EPR Spectroscopy. [(*p*-TTP)Fe(2,6-xylylNC)$_2$]CF_3SO_3 (**1**) and [(TPP)Fe(2,6-xylylNC)$_2$]CF_3SO_3 (**2**) exhibit identical axial EPR spectra, with *g* values of $g_\perp = 2.2$ and $g_{||} = 1.94$ (Figure 5a). These values are identical with those reported for [(TPP)-Fe(*t*-BuNC)$_2$]ClO_4,[17] which also exhibits the $(d_{xz},d_{yz})^4(d_{xy})^1$ ground state. Assuming this ground state, the mixing coefficients *a*, *b*, and *c* of the Fe d_{yz}, d_{xz}, and d_{xy} atomic orbitals, respectively, can be calculated from the *g* values[22] according to

$$\begin{aligned} g_{xx} &= 2[a^2 - (b + c)^2] \\ g_{yy} &= 2[(a + c)^2 - b^2] \\ g_{zz} &= 2[(a + b)^2 - c^2] \\ a^2 + b^2 + c^2 &= 1 \end{aligned} \tag{3}$$

(82) Simonneaux, G. *Coord. Chem. Rev.* **1997**, *165*, 447.

Table 4. Rhombicity and Tetragonality Parameters as Obtained from the EPR Data According to Eq 4

	2 and **1**	**3**
V/λ	0	0
Δ/λ	−8.90	−
% d_{xy}	98%	100%

We follow the convention that the heme normal is the *z*-axis.[23] The *g* values can be used to calculate the relative energies of the Fe formerly t_{2g} orbitals and their tetragonal (Δ/λ) and rhombic (V/λ) splitting parameters,[23] in terms of the spin−orbit coupling constant λ, according to

$$V/\lambda = \frac{g_x}{g_z + g_y} + \frac{g_y}{g_z - g_x}$$
$$\Delta/\lambda = \frac{g_x}{g_z + g_y} + \frac{g_z}{g_y - g_x} - \frac{1}{2} V/\lambda \quad (4)$$

The parameters calculated in this way are listed in Table 4. The EPR spectrum only provides the absolute values of the diagonal elements of the *g*-tensor. The *g*-tensor consistent with a $(d_{xz},d_{yz})^4(d_{xy})^1$ ground state is $\bar{\bar{g}} = (-2.2, 2.2, -1.94)$ according to eqs 3.

The [(*m*-TTP)Fe(2,6-xylylNC)$_2$]CF$_3$SO$_3$ complex (**3**) exhibits an isotropic EPR signal at $g = 2.14$ in the solid state. The EPR spectra of CH_2Cl_2 frozen solutions of complexes **1**, **2**, and **3** all show axial EPR signals with $g_\perp = 2.15-2.18$ and $g_\parallel = 1.94-1.95$ (data not shown). The difference between solution- and solid-state EPR spectra of the porphyrin complex **3** may be caused by a slightly different structure in the solid state than in solution, or, more likely, it may be a result of exchange narrowing due to spin−spin interactions in the solid state. On the basis of the NMR data discussed above, we have found that the ground states of all three complexes are of the d_{xy} type. This is supported by the fact that the EPR spectra of their CH_2Cl_2 frozen solutions are almost identical. Therefore, based on the strong evidence from the NMR and the frozen solution EPR spectra of complex **3**, we assume the *g*-tensor to be $\bar{\bar{g}} = (-2.14, 2.14, -2.14)$, which is consistent with a d_{xy} HOMO.

Mössbauer Spectroscopy. The Mössbauer spectrum of [(TPP)Fe(2,6-xylylNC)$_2$]CF$_3$SO$_3$ (**2**) obtained at 190 K in an applied field of 20 mT is shown in Figure 6a. At 4.2 K, also at 20 mT, basically the same magnetically broadened asymmetric doublet is observed, with an isomer shift of $\delta = 0.08$ mm/s and a quadrupole splitting $|\Delta E_Q| = 1.99$ mm/s (Figure 6b). This lack of change with temperature is explained by the fact that temperature-independent spin−spin relaxation is reflected in the Mössbauer spectra. To slow the spin−spin relaxation rate, spectra were collected at 4.2 K in fields of up to 5.34 T parallel and perpendicular to the γ-beam; representative spectra are displayed in Figure 6c−e. It should be noted that no consistent hyperfine parameter set could be found to simulate the spectra shown in Figure 6 according to eq 2, assuming either slow or fast relaxation limits. Even extensive variation of the Euler angles that describe the rotation from the principal axis of $\bar{\bar{g}}$ and $\bar{\bar{A}}$ to the axis of the efg tensor, a method used successfully for dissolved [(TPP)Fe(*t*-BuNC)$_2$]ClO$_4$,[17] did not reproduce the Mössbauer pattern.

Since relaxation effects influence the Mössbauer spectra under all conditions applied, they have been analyzed by using the dynamic line shape formalism of Blume and Clauser.[63,64] The solid lines shown in Figure 6 are spin-Hamiltonian simulations for an $S = {}^1/_2$ system with the parameters given in Table 5 and spin relaxation rates given in the caption of Figure 6. The negative sign of the quadrupole splitting, $\Delta E_Q = -1.99$ mm/s, is indicative of a singly occupied d_{xy} HOMO, which confirms the analysis of the EPR spectra. As already discussed above, the Griffith model yields for this situation the *g*-tensor $\bar{\bar{g}} = (-2.2, 2.2, -1.94)$. The *g*-tensor thus obtained was used to simulate the Mössbauer spectra in Figure 6, and an experimental *A*-tensor of $\bar{\bar{A}}/g_N\mu_N = (-5.5, 5.5, 40)$ T was found.

As reported by Lang, it is possible to calculate the *A*-tensor from the expressions[83−85]

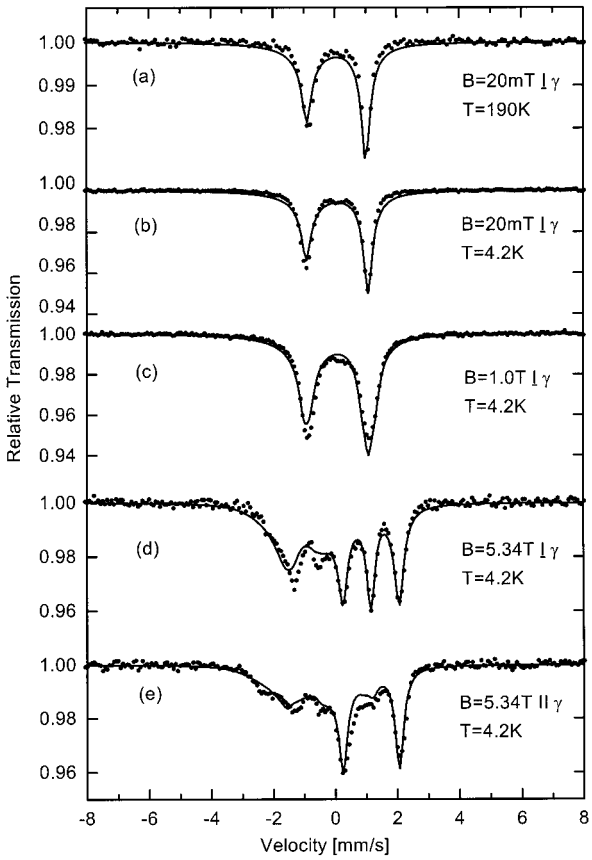

Figure 6. Mössbauer spectra of [(TPP)Fe(2,6-xylylNC)$_2$]CF$_3$SO$_3$ (**2**) obtained at (a) 190 K and 4.2 K in fields of (b) 20 mT, (c) 1 T, and (d) 5.34 T perpendicular to the γ-beam, as well as in a field of 5.34 T parallel to the γ-beam (e). The solid lines are simulations with the spin-Hamiltonian parameters given in Table 5 and the relaxation rates (a, b) 2.2×10^8 s^{-1}, (c) 1.9×10^8 s^{-1}, and (d, e) 6.0×10^7 s^{-1}.

Table 5. Mössbauer[a] and Spin-Hamiltonian Parameters Obtained from the Simulations Shown in Figures 6, 8, and 9

	$\bar{\bar{g}}$	δ (mm/s)	ΔE_Q (mm/s)	Γ (mm/s)	η	$\bar{\bar{A}}/g_N\mu_N$ (T)
1	(−2.2, 2.2, −1.94)	0.14	−1.81	0.26	0	(−5.5, 5.5, 27)
2	(−2.2, 2.2, −1.94)	0.08	−1.99	0.26	0	(−5.5, 5.5, 40)
3	(−2.14, 2.14, −2.14)	0.12	±1.94[b]	0.26	1	(−2.5, 2.5, 32)

[a] The spectrum of [(TPP)Fe(2,6-xylylNC)$_2$]CF$_3$SO$_3$ (**2**) obtained at 190 K (Figure 6a) has been analyzed with $\delta = 0.05$ mm/s and $\Delta E_Q = -1.90$ mm/swith all other parameters as quoted in the table. That of [(*p*-TTP)Fe(2,6-xylylNC)$_2$]CF$_3$SO$_3$ (**1**) (Figure 8a) has been analyzed with $\delta = 0.10$ mm/s and $\Delta E_Q = -1.76$ mm/s and that of [(*m*-TTP)Fe(2,6-xylylNC)$_2$]CF$_3$SO$_3$ (**3**) (Figure 9a) with $\delta = 0.10$ mm/s and $\Delta E_Q = \pm 1.75$ mm/s.[b] [b] The sign of the quadrupole splitting cannot be determined since $\eta = 1$.

(83) Oosterhuis, W. T.; Lang, G. *J. Chem. Phys.* **1969**, *50*, 4381.
(84) Oosterhuis, W. T.; Lang, G. *Phys. Rev.* **1969**, *178*, 439.
(85) Rhynard, D.; Lang, G.; Spartalian, K.; Yonetani, T. *J. Chem. Phys.* **1979**, *71*, 3715.

$$A_x = -P\Big[-4bc - (1+k)(a^2 - b^2 - c^2) + \frac{3}{7}(a^2 - 3b^2 - 3c^2) + \frac{6}{7}a(b+c)\Big]$$

$$A_y = +P\Big[-4ac - (1+k)(b^2 - a^2 - c^2) + \frac{3}{7}(b^2 - 3a^2 - 3c^2) + \frac{6}{7}b(a+c)\Big] \quad (5)$$

$$A_z = +P\Big[-4ab - (1+k)(c^2 - a^2 - b^2) + \frac{3}{7}(c^2 - 3a^2 - 3b^2) + \frac{6}{7}c(a+b)\Big]$$

The proportionality constant P is taken as -62 T and the Fermi contact constant $\kappa = 0.35$ as for most heme proteins[86] and heme models.[9]

If one calculates the A-tensor according to this model one obtains $\bar{A}/g_N\mu_N = (-7.4, 7.4, 50.9)$ T. The experimental values quoted above are reduced with respect to the calculated values (eqs 5) by approximately 25%, which may be caused by covalency effects in the iron−ligand bonds and/or spin delocalization by porphyrin → Fe π donation.[24]

The relaxation process can be identified as follows: The population $P(m_s = +^1/_2)$ of the upper $m_s = +^1/_2$ Zeeman level is given by the Boltzmann factor,

$$P(m_s = +^1/_2) = \frac{\exp(-\Delta E/k_B T)}{1 + \exp(-\Delta E/k_B T)} \quad (6)$$

with the Zeeman energy

$$\Delta E = g\mu_B B \quad (7)$$

Figure 7 shows a linear relationship of the relaxation rates obtained from the Mössbauer analysis as a function of $P(m_s = +^1/_2)$ for the different applied fields. This linear relationship is characteristic for spin−spin relaxation, or to be more specific, cross relaxation,[87] because the probability for the latter rises linearly with the occupation of the upper level at one of the neighboring ions. Thus, this situation can only arise in a concentrated sample such as a polycrystalline solid sample of a low-spin iron(III) porphyrinate and is not expected to occur for either frozen solutions of ^{57}Fe-enriched samples of ferriheme models and proteins or polycrystalline heme proteins, where the hemes are well separated from each other.

The Mössbauer spectra of [(*p*-TTP)Fe(2,6-xylylNC)$_2$]CF_3SO_3 (**1**), obtained at 190 and 4.2 K in fields of 20 mT and 5.34 T, are shown in Figure 8. The solid lines are spin-Hamiltonian simulations with the parameters given in Table 5. The spectra have been analyzed with the relaxation rates corresponding to those used for [(TPP)Fe(2,6-xylylNC)$_2$]CF_3SO_3 (**2**). Again, the negative sign of the quadrupole splitting, $\Delta E_Q = -1.81$ mm/s, is indicative of a singly occupied d_{xy} HOMO. The experimental A-tensor is $\bar{A}/g_N\mu_N = (-5.5, 5.5, 27)$ T. A_z is reduced from the theoretical value of 50.9 T by approximately 50%, indicating that the covalency effects in [(*p*-TTP)Fe(2,6-xylylNC)$_2$]CF_3SO_3 (**1**) are more important than those in [(TPP)Fe(2,6-xylylNC)$_2$]-CF_3SO_3 (**2**).

The Mössbauer spectra of [(*m*-TTP)Fe(2,6-xylylNC)$_2$]CF_3-SO_3 (**3**) obtained at 4.2 K in fields of 20 mT and 5.34 T are shown in Figure 9. The solid lines are spin-Hamiltonian simulations with the parameters given in Table 5. The spectra have been analyzed with relaxation rates corresponding to those used for [(TPP)Fe(2,6-xylylNC)$_2$]CF_3SO_3 (**2**) and [(*p*-TTP)Fe-(2,6-xylylNC)$_2$]CF_3SO_3 (**1**). The magnetic Mössbauer pattern of Figure 9b can best be simulated by taking the asymmetry parameter $\eta = 1$. Therefore, we cannot determine the sign of the quadrupole splitting for complex **3**. A pure d_{xy} hole would exhibit $\eta = 0$, as in the cases of complexes **1** and **2**. However, the complex [(OEP)Fe(*t*-BuNC)$_2$]ClO_4 exhibits $\eta = 0.41$ in the solid state, but an almost zero asymmetry parameter of $\eta = 0.14$ in solution.[17] The reason for the increase in the asymmetry parameter in the solid state is not clear. The ruffling of the porphyrin plane present in [(OEP)Fe(*t*-BuNC)$_2$]ClO_4 and probably also in complex **3** may lead to strong delocalization of the d_{xy} iron hole to the p_z orbitals of the porphyrin nitrogens via the $a_{2u}(\pi)$ filled porphyrin orbital, but whether this admixture can lead to such strong changes of η may be questionable. This

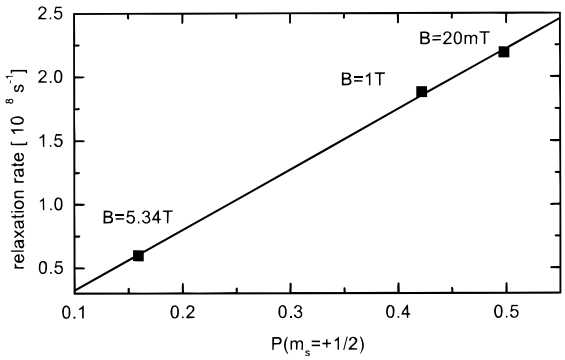

Figure 7. Relaxation rates obtained from the Mössbauer analysis of [(TPP)Fe(2,6-xylylNC)$_2$]CF_3SO_3 (**2**) (Figure 6) as a function of the Boltzmann population of the upper Zeeman level $P(m_s = +^1/_2)$ calculated from eq 6 for the different indicated applied fields.

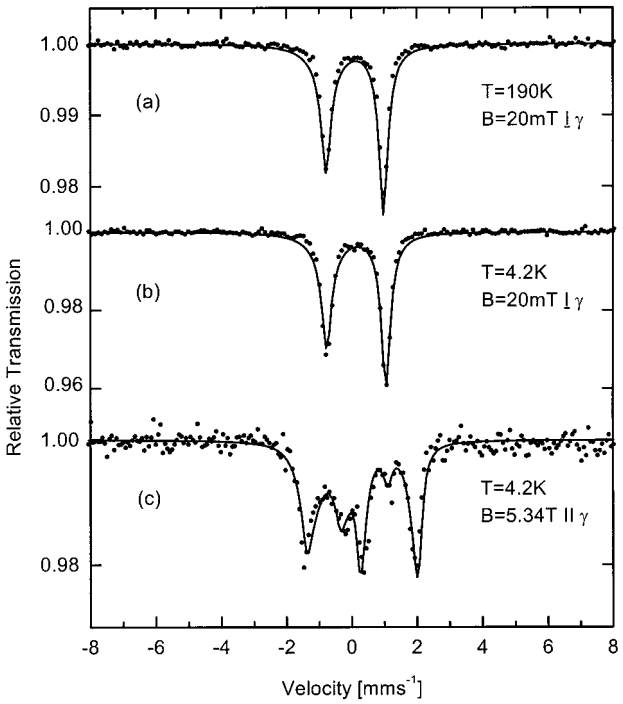

Figure 8. Mössbauer spectra of [(*p*-TTP)Fe(2,6-xylylNC)$_2$]CF_3SO_3 (**1**) obtained at (a) 190 K and 4.2 K in fields of (b) 20 mT and (c) 5.34 T parallel to the γ-beam. The solid lines are simulations with the spin-Hamiltonian parameters given in Table 5 and the relaxation rates 2.2 $\times$ 10^8 s^{-1} for (a) and (b) and 6.0 $\times$ 10^7 s^{-1} for (c).

(86) Lang, G. *Q. Rev. Biophys.* **1970**, *3*, 1.
(87) Boyle, A. J. F.; Gabriel, J. R. *Phys. Lett.* **1965**, *19*, 451.

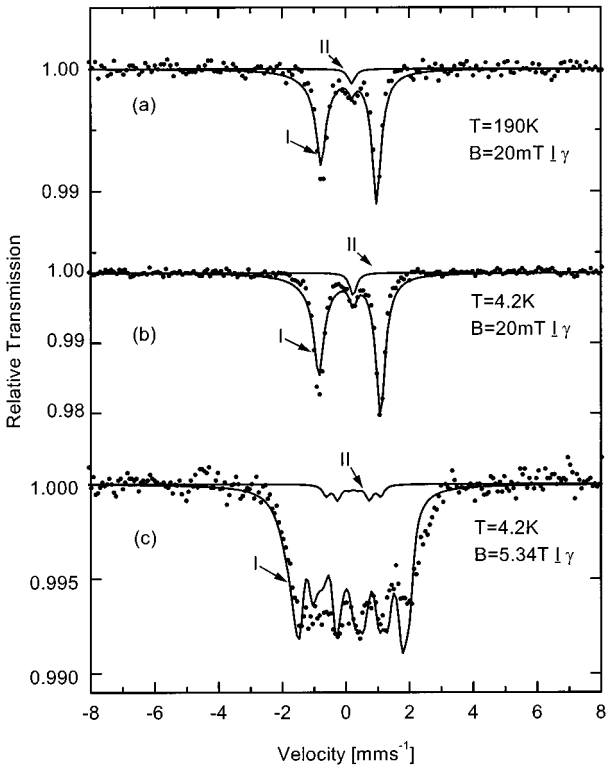

Figure 9. Mössbauer spectra of [(*m*-TTP)Fe(2,6-xylylNC)$_2$]CF$_3$SO$_3$ (**3**) obtained at (a) 190 K and at 4.2 K in fields of (b) 20 mT and (c) 5.34 T perpendicular to the γ-beam. The solid lines for subspectra I are simulations with the spin-Hamiltonian parameters given in Table 5 and the relaxation rates 2.2×10^8 s^{-1} for (a) and (b) and 6.0×10^7 s^{-1} for (c). Subspectrum II exhibits $\delta = 0.24$ mm/s at 4.2 K in (b) and $\delta = 0.19$ mm/s at 190 K in (a), as well as $\Delta E_Q = 0$ mm/s and $\Gamma = 0.26$ mm/s and was simulated in (c) assuming $S = 0$; it accounts for 4% of the total area and is attributed to ferrous low-spin [(*m*-TTP)Fe-(2,6-xylylNC)$_2$] caused by autoreduction of the ferric form.

may be addressed further by molecular orbital calculations once the structure of **3** has been solved. Nevertheless, the Mössbauer spectra have been measured in the solid state, and therefore we have used for the analysis reported here the *g*-factors measured for the solid complex **3**, $\bar{\bar{g}} = (-2.14, 2.14, -2.14)$. From these, the theoretical *A*-tensor according to eq 5 follows as $\bar{\bar{A}} = (-4.2, 4.2, 61.1)$ T. The experimental *A*-tensor is $\bar{\bar{A}}/g_N\mu_N = (-2.5, 2.5, 32)$ T. As for complexes **1** and **2**, this deviation of about 50% is also attributed to covalency effects.

The NMR analysis discussed above and shown in Figure 4 indicates that the complexes under investigation exhibit a relatively low-lying excited state, presumably the $(d_{xz},d_{yz})^3(d_{xy})^2$ state, at some energy above the $(d_{xz},d_{yz})^4(d_{xy})^1$ ground state. Low-lying states may influence the relaxation behavior of paramagnetic centers via Orbach-like spin−lattice relaxation processes. Such processes exhibit a relaxation behavior that is field independent but strongly temperature dependent. The Mössbauer analysis of the solid iron porphyrinates presented in this study clearly shows that a field-dependent and temperature-independent relaxation process is effective at 4.2 K. The mechanism is identified above as spin−spin or cross relaxation. This type of relaxation process, however, is not influenced by low-lying excited crystal field states. However, at higher temperatures, the quadrupole splitting, ΔE_Q, may vary if an excited state is populated, if the quadrupole splitting of that excited state is opposite in sign to that of the ground state. In fact, according to the Townes−Dailey approximation, for a single unpaired electron in the d_{xy} orbital, a negative sign for

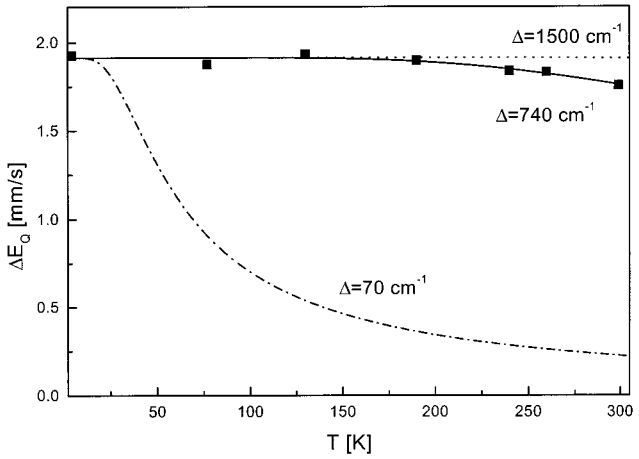

Figure 10. Temperature dependence of the quadrupole splitting of [(TPP)Fe(2,6-xylylNC)$_2$]CF$_3$SO$_3$ (**2**). The solid line has been calculated according to eq 4 with $\Delta E = 740$ cm^{-1}, the dash−dotted line with $\Delta E = 70$ cm^{-1}, and the dotted line with $\Delta E = 1500$ cm^{-1}.

Table 6. Magnitude Per d Electron of the Diagonal Electric Field Gradient (efg)$_{val}$ Tensor Elements[a]

orbital	$(V_{xx})_{val}/e\langle r^{-3}\rangle$	$(V_{yy})_{val}/e\langle r^{-3}\rangle$	$(V_{zz})_{val}/e\langle r^{-3}\rangle$
d_{xy}	−2/7	−2/7	+4/7
d_{xz}	−2/7	+4/7	−2/7
d_{yz}	+4/7	−2/7	−2/7
$d_{x^2-y^2}$	−2/7	−2/7	+4/7
d_{z^2}	+2/7	+2/7	−4/7

[a] Note that for a hole the signs of $\langle V_{ii}\rangle/e<r^{-3}>$ reverse.

ΔE_Q is expected, while for a single unpaired electron in either d_{xz} or d_{yz}, a positive sign for ΔE_Q is expected. Thus, population of an excited state with an unpaired electron in d_{xz} or d_{yz} should cause a decrease in the magnitude of the observed quadrupole splitting.

Figure 10 shows the temperature dependence of the quadrupole splitting of [(TPP)Fe(2,6-xylyl)$_2$]CF$_3$SO$_3$ (**2**) in the range from 4.2 to 300 K. The simulations of the spectra obtained at 4.2 K in high magnetic fields yield a negative sign of the quadrupole splitting, which is consistent with a d_{xy} electronic ground state. Since the rhombicity, *V*, of **1**, **2**, and **3** has been determined to be zero from the EPR analysis, the first excited state represents a hole either in the d_{yz} or in the d_{xz} orbital, which means that the first excited state is doubly degenerate. Thermal population of the doubly degenerate excited state leads to a decrease in the overall quadrupole splitting, if one assumes fast relaxation (or almost fast, as in our case), because the excited states with the hole in a d_{yz} or d_{xz} orbital exhibit a positive quadrupole splitting.

To calculate the temperature dependence of ΔE_Q, we assume that the electric field gradient (efg) tensor has only orbital contributions. If we denote the efg tensor originating from a hole in a d_{xy}, d_{xz}, and d_{yz} orbital as $\bar{\bar{V}}_{xy}$, $\bar{\bar{V}}_{xz}$, and $\bar{\bar{V}}_{yz}$ and consider that the d_{xz} and d_{yz} excited states are degenerate, twice the temperature dependence of the efg tensor $V(T)$ is given by

$$\bar{\bar{V}}(T) = \frac{1}{Z}(\bar{\bar{V}}_{xy} + \bar{\bar{V}}_{xz}\, e^{-\Delta E/k_B T} + \bar{\bar{V}}_{yz}\, e^{-\Delta E/k_B T}) \qquad (8)$$

with *Z* being the statistical sum $Z = 1 + 2e^{-\Delta E/k_B T}$ for a three-level system with a degenerate excited state separated from the ground state by ΔE. Insertion of the expectation values $\langle V_{ii}\rangle/e\langle r^{-3}\rangle$ (see Table 6) into eq 8 yields

$$\vec{\vec{V}}(T)/e\langle r^{-3}\rangle = \frac{\begin{pmatrix} \frac{2}{7} & & \\ & \frac{2}{7} & \\ & & -\frac{4}{7} \end{pmatrix} + \begin{pmatrix} -\frac{4}{7} & & \\ & \frac{2}{7} & \\ & & \frac{2}{7} \end{pmatrix} \cdot e^{-\Delta E/k_B T} + \begin{pmatrix} +\frac{2}{7} & & \\ & -\frac{4}{7} & \\ & & \frac{2}{7} \end{pmatrix} \cdot e^{-\Delta E/k_B T}}{1 + 2e^{-E/k_B T}}$$

$$= \frac{\begin{pmatrix} \frac{2}{7} & & \\ & \frac{2}{7} & \\ & & -\frac{4}{7} \end{pmatrix} + \begin{pmatrix} -\frac{2}{7} & & \\ & -\frac{2}{7} & \\ & & \frac{4}{7} \end{pmatrix} \cdot e^{-\Delta E/k_B T}}{1 + 2e^{-E/k_B T}} \qquad (9)$$

The quadrupole splitting $\Delta E_Q(T)$ is proportional to the main component $V_{zz}(T)$ of the efg tensor:

$$E_Q(T) \sim V_{zz}(T)\sqrt{1 + \eta(T)^2/3} \qquad (10)$$

Insertion of the efg elements obtained in eq 8 gives in the present case $\eta(T) = 0$ for all temperatures. Therefore, ΔE_Q is proportional to V_{zz}, and combining eqs 9 and 10 yields, for the temperature dependence of the electronic contribution to ΔE_Q:

$$\Delta E_Q(T) = \frac{\exp(-\Delta E/k_B T) - 1}{2\exp(-\Delta E/k_B T) + 1}\,\Delta E_Q(4.2\text{ K}) \qquad (11)$$

The solid and dashed lines in Figure 10 have been calculated from eq 11 using $\Delta E = 740$ cm^{-1} and $\Delta E = 70$ cm^{-1}, the limiting values derived from the temperature dependence of the NMR spectra. For comparison, we also show the dotted line which corresponds to $\Delta E = 1500$ cm^{-1} as an upper limit. Clearly, the value for $\Delta E = 740$ cm^{-1} fits the temperature dependence of the quadrupole splitting well.

The energy difference ΔE should correspond to the crystal field splitting Δ, which has been calculated from the electronic *g*-tensors (see Table 4). If we set $\Delta E = \Delta = 740$ cm^{-1} and insert the value of $\Delta/\lambda = 8.90$ obtained for complex **2** (Table 4), we obtain $\lambda = 83$ cm^{-1}. This value is much lower than the free ion value (460 cm^{-1}).[88] Nevertheless, for K_3FeCN_6 a value of $\lambda = 80 \pm 5$ cm^{-1} was determined experimentally by a combined EPR, NMR, and Mössbauer study.[89] However, Bleaney et al. used 278 cm^{-1} in the interpretation of their EPR data for K_3FeCN_6,[90] and Figgis et al. reported 275−375 cm^{-1},[91] the range of the latter values being consistent with MO calculations performed by Reschke et al.[92] Maltempo has used the value of 300 cm^{-1} for low-spin ferrihemes,[93] while Levin and Brill obtained a value of 350 cm^{-1} for metmyoglobin complexes.[94] Walker and co-workers have previously used 400 cm^{-1} as the maximum possible value of λ for low-spin ferrihemes having the $(d_{xy})^2(d_{xz},d_{yz})^3$ electronic ground state,[7] Horrocks and Greenberg[95] have used 340 cm^{-1}, and Turner and co-workers[96] have used 270 cm^{-1} for the same types of systems. The MO calculations[92] show that covalency effects indeed lead to a reduction of λ from the free ion value. Thus, covalency certainly plays a role for the complexes studied here. However, we believe that its importance, as suggested by the low value of $\lambda = 83$ cm^{-1}, is greatly overestimated; rather, a value 2−4 times this is more reasonable, based upon previous work.[90−96] Thus, we expect the crystal field value Δ to be of the order of 1500−3000 cm^{-1}, perhaps nearer the smaller to emphasize the importance of covalency. Therefore, the temperature dependence of the quadrupole splitting must be attributed to effects other than Boltzmann population of excited orbital states, i.e., to dynamic effects.

Such dynamic effects as rotation of axial ligands at higher temperatures have previously been observed in low-spin ($S = 0$) Fe(II) porphyrins.[97,98] However, the axial ligands of this study have cylindrical symmetry at the binding site to the metal, and it is very unlikely that rotation of the xylyl groups would in any way affect the energies of the orbitals of the metal center. Furthermore, the samples of this study are polycrystalline solids, in which large-scale motions of parts of the molecule are prevented by the packing in the crystalline lattice. However, the strongly ruffled porphyrin ring, which is stabilized in the ruffled conformation by porphyrin-to-metal π donation from the $3a_{2u}(\pi)$ orbital to the hole in the metal d_{xy} orbital,[11] should have an associated low-energy "inversion" of the ruffled ring. Such an "inversion" is clearly observed when bulky planar axial ligands are present on tetramesitylporphyrinatoiron(III), for it is required for their rotation.[99−101] And even in the absence of planar axial ligands, such "inversion" must occur and should be a relatively low-energy process. This "inversion" would move *meso* positions that are displaced above the mean plane of the porphyrin ring shown in Figure 2 down, while those displaced below the mean plane are moved up, with concomitant lengthening of the Fe−N(por) bonds at the planar transition state. Although such large-scale movements from one ruffled conformation to the other are unlikely in the solid state, a partial "inversion," in which the porphyrin ring approaches planarity, with Fe−N(por) bonds lengthened, may be possible. From what has been learned about ruffled vs planar porphyrin rings in this and previous work, it is reasonable to expect that the planar porphyrin ring would stabilize the unpaired electron in the d_{xz},d_{yz} orbitals, yielding a $(d_{xy})^2(d_{xz},d_{yz})^3$ electron configuration for this transition state, the same electron configuration as expected for the excited electronic state of the ruffled conformation, discussed

(88) Figgis, B. N.; Lewis, J. In *Techniques of Inorganic Chemistry*; Jonassen, H. B., Weiss- berger, A., Eds.; Weiley Interscience: New York, 1965; Vol. IV, p 159.
(89) Merrithew, P. B.; Modestino A. J. *J. Am. Chem. Soc.* **1972**, *94*, 3361.
(90) Bleany, B.; O'Brien, *Proc. Phys. Soc.* **1956**, *B69*, 1216.
(91) Figgis, B. N.; Gerlach, M.; Mason, B. *Proc. R. Soc.* **1969**, *A309*, 91.
(92) Reschke, R.; Trautwein A.; Harris, F. E.; Date, S. K. *J. Magn. Magn. Mater.* **1979**, *12*, 176.
(93) Maltempo, M. M. *J. Chem. Phys.* **1974**, *61*, 2540.
(94) Levin, P. D.; Brill, A. S. *J. Phys. Chem.* **1988**, *92*, 5103.
(95) Horrocks, W. DeW.; Greenberg, E. S. *Biochim. Biophys. Acta* **1973**, *322*, 38; *Mol. Phys.* **1974**, *27*, 993.
(96) Turner, D. L. *Eur. J. Biochem.* **1993**, *211*, 563.
(97) Schappacher, M.; Ricard, L.; Fischer, J.; Weiss, R.; Bill, E.; Montiel-Mantoya, R.; Winkler, H.; Trautwein, A. X. *Eur. J. Biochem.* **1987**, *168*, 419.
(98) Grodzicki, M.; Flint, H.; Winkler, H.; Walker, F. A. Trautwein, A. X. *J. Phys. Chem. A* **1997**, *101*, 4202.
(99) Walker, F. A.; Simonis, U. *J. Am. Chem. Soc.* **1991**, *113*, 8652; **1992**, *114*, 1929.
(100) Shokhirev, N. V.; Shokhireva, T. Kh.; Polam, J. R.; Watson, C. T.; Raffii, K.; Simonis, U.; Walker, F. A. *J. Phys. Chem. A* **1997**, *101*, 2778.
(101) Polam, J. R.; Shokhireva, T. Kh.; Raffii, K.; Simonis, U.; Walker, F. A. *Inorg. Chim. Acta* **1997**, *263/1−2*, 109.

in the previous paragraph. Thus, such a partial "inversion" in the solid state, and a complete "inversion" in solution, provide an explanation for the temperature dependence of the quadrupole splitting in the solid state and the isotropic shifts of the porphyrinate protons in homogeneous solution. It also allows for a different (lower) barrier to inversion of the ruffled porphyrinate ring in solution than in the solid state, consistent with the fact that the lower value of $\Delta E \approx 70$ cm^{-1} appears to fit the NMR data better (Figure 4), while a much higher value of $\Delta E \approx -740$ cm^{-1} fits the Mossbauer data better (Figure 10).

It is interesting to note that a too-small value of $\Delta E \approx 296$ cm^{-1} was found and commented on from the temperature dependence of the isotropic shifts of [(OEP)Fe(*t*-BuNC)$_2$]$^+$, for which the tetragonal splitting Δ/λ was found to be -8.33, similarly suggesting a value of Δ in the range of 1500$-$3000 cm^{-1}.[17] It is now possible to conclude with some confidence that in that case, as in the present complexes **1**$-$**3**, porphyrin "inversion" is undoubtedly responsible for the small value of ΔE, and that this energy term represents an activation energy for reaching the planar transition state of the ruffled complex.

Acknowledgment. The financial support of the MESR (C.M.), the Deutsche Forschungsgemeinschaft (A.X.T.), and the National Institutes of Health (USA), DK31038 (F.A.W.), is gratefully acknowledged.

Supporting Information Available: Figures showing an ORTEP drawing of the porphyrinate cation and anion of **1** and the packing diagram and unit cell of **1**, and four tables showing the bond distances, bond angles, positional parameters, and displacement parameters for **1** (PDF). This material is available free of charge via the Internet at http://pubs.acs.org.

JA994190T